Chalcogenisation of Cu-Sb Metallic Precursors into $Cu_3Sb(Se_xS_{1-x})_3$

Pietro Maiello*, Guillaume Zoppi, Robert W. Miles, Nicola Pearsall and Ian Forbes

Northumbria Photovoltaics Applications Centre, Northumbria University, Ellison Building, Newcastle upon Tyne, NE1 8ST, UK

*Corresponding author. Tel.: +44 0191 243 7013

E-mail address: pietro.maiello@northumbria.ac.uk

Abstract

Cu_3SbS_3 is a novel chalcogenide semiconductor with p-type conductivity and an energy bandgap of 1.84eV. By incorporating selenium into this material to form $Cu_3Sb(Se_xS_{1-x})_3$ where x=Se/(Se+S), the energy bandgap can be altered to be in the range 1.38-1.84 eV for $0<x<0.49$. The energy bandgap can hence be adjusted to be near the optimum for making the absorber layer for use in single and multi-junction photovoltaic solar cell devices. In this paper these materials were prepared using a two-stage process that involved magnetron sputtering of the Cu-Sb precursor layers followed by conversion to Cu_3SbS_3 by annealing in the presence of elemental sulphur and to $Cu_3Sb(S_xSe_{1-x})_3$ by annealing in the presence of a mixture of sulphur and selenium. The films synthesised were characterised using scanning electron microscopy, energy dispersive x-ray analysis, x-ray diffraction, secondary ion mass spectroscopy and photo-electrochemical measurements. When the Cu_3SbS_3 was formed on glass substrates it had a cubic crystal structure whereas when it was formed on Mo-coated glass it had the monoclinic crystal structure. Likewise the layers of $Cu_3Sb(S,Se)_3$ formed on Mo-coated glass also had the monoclinic crystal structure. Spectral response curves were recorded over the spectral range 400-1400 nm for semiconductor – electrolyte junctions. Photovoltaic solar cell devices were made using p-type $Cu_3Sb(S_xSe_{1-x})_3$ as the absorber layer and n-type CdS as the buffer layer. The photovoltaic effect was observed in these devices.

Keywords: thin films, $Cu_3Sb(S,Se)_3$, sulfurization, selenization, photovoltaics

1. Introduction

The current thin film photovoltaics (PV) market is dominated by technologies based on the use of cadmium telluride (CdTe), $CuInGaSe_2$ (CIGS) and hydrogenated amorphous silicon a-Si:H [1]. In the last decade, considerable improvements have been achieved for devices based on CIGS absorbers,

both in the laboratories and manufacturing plants. Indeed, CIGS solar cells have been made with laboratory efficiencies up to 20.3% [2]. However, the ability of these technologies to meet the predicted multi-TW PV market later this century may be limited by the scarcity and high cost of In and Te in CIGS and CdTe, respectively [3, 4]. There is an urgent need for new light absorbing semiconductors made from more abundant elements that can be used to make high efficiency devices. There are a large number of metal chalcogenide semiconductors which exhibit opto-electronic properties that are suitable for photovoltaic applications [5, 6]. It should also be noted that making tandem thin film solar cell devices should lead to a significant increase in device efficiencies. Modelling calculations based on a two solar cells tandem system, estimate that efficiencies of approximately 38% can be achieved using semiconductors with an energy bandgap of 1.5-1.85 eV for the bottom subcell and 0.85-1.3 eV for the top subcell under the air mass (AM) 1.5 spectrum [7, 8]. Therefore, new materials that offer the opportunity to vary the energy bandgap are of interest for making multijunction devices.

Thin film chalcogenides of Cu-Sb have been investigated by a number of groups [9-14]. These studies have mainly considered compounds with the $CuSbS_2$ and $CuSbSe_2$ stoichiometries, with energy bandgap values of 1.5 and 1.2 eV, respectively [9]. In our previous work on the sulphurisation of Cu-Sb precursors libraries [15], a stable Cu_3SbS_3 stoichiometry was identified for the first time as thin film. The present work reports on its structural, morphological and electronic properties as a function of sulphurisation condition and its alloy with Se.

2. EXPERIMENTAL

2.1 Film Processing

The Cu-Sb metallic precursors were deposited by direct current (DC) magnetron sputtering from 7.6 cm diameter, high purity (99.999%) targets onto bare or molybdenum coated soda-lime glass (SLG) substrates with the following dimensions: 76 mm x 26 mm x 1 mm. The base pressure in the deposition system was $<5x10^{-7}$ mbar prior to deposition and high purity argon (99.998%) was used as the ionizing gas.

Precursors were chalcogenised in closed graphite boxes placed inside a tube furnace at temperature up to 550 °C and under 1 mbar argon pressure. The samples were heated at a rate of 20 °C/min, followed by a dwell time of 30 min, before being left to cool to room temperature. Sulphurisation of the precursors was achieved using elemental S powder or an evaporated S layer. In the first case, elemental sulphur powder was uniformly distributed onto the surface of the metallic precursors and heated to temperatures of 250-550 °C (in steps of 50 °C). Combined S and Se chalcogenisation took

place by evaporating S and Se layers onto the precursors before placing them in a graphite box and then annealing at 500 °C. With these methods $Cu_3Sb(Se_xS_{1-x})_3$ thin films were produced, where x=Se/(Se+S). Selected samples were incorporated into conventional Ni-Al/ITO/i-ZnO/CdS/absorber/Mo/Glass-device structures (Indium-Tin-Oxide=ITO), using chemical bath deposited CdS and sputtered ITO/i-ZnO bilayers.

2.2 Materials characterisation

The morphology and composition of the converted layers were investigated using a scanning electron microscopy (SEM, FEI Quanta 200). Quantitative energy dispersive x-ray spectroscopy (EDS) measurements were made using a lithium-drifted silicon detector attached to the SEM. Crystallographic properties were analysed by x-ray diffraction (XRD) using a Bruker D5000 diffractometer in the θ-2θ geometry using 1.5406 Å Cu-Kα radiation. Depth profiling and lateral uniformity of the layers were investigated by secondary ion mass spectroscopy (SIMS) using a Hiden Analytical 4 keV Ar^+ ion gun and quadrupole mass detector. The rastered area was 500 μm x 500 μm and the gated area was 10%.

2.3 Electrical and Optoelectronic Characterisation.

To examine the performance of the absorber layers as part of a functioning cell whilst minimising the need to optimise full device processing a liquid electrolyte was used to form the contact and junction. The subsequent photoelectrochemical measurements were performed using a potentiostat (Sycopel Scientific) in a 3 electrode glass cell with an Ag/AgCl reference electrode and a platinum wire counter electrode in an aqueous europium solution (0.2 M in $Eu(NO_3)_3 \cdot 6\ H_2O$). Constant potential photocurrent transients indicative of photo-activity were produced using pulsed white light from a modulated LED (light emitting diode) [16]. From the electrolyte/absorber junctions photocurrent spectra of the semiconducting films were measured using a tungsten lamp, mono-chromator, optical chopper, lock-in amplifier (Bentham) and potentiostat. Spectra were recorded at a chopping frequency of 75Hz. The intensity of the signal was maximised by adjusting the potential between the reference electrode and the sample. External quantum efficiency (EQE) curves were determined using calibrated silicon and germanium photodiodes. The conductivity type of the films was determined using the hot probe method for the films deposited on glass and the pulsed white light technique described above for the films deposited on Mo/glass. Solar photovoltaic devices were also produced and open circuit voltage/short circuit current values were measured for the photo-active cellsunder standard conditions (Class A, AM1.5, 100 mW/cm^2, 25 °C).

3. RESULTS AND DISCUSSION

3.1 Cu-Sb precursors

The precursor films sputtered on either glass or Mo/glass substrates had an atomic composition of 68% Cu and 32% Sb and thickness of 380 nm. The corresponding XRD pattern of such a metallic film deposited on Mo/glass is shown in Figure 1. This indicates the presence of a binary alloy, which matched with the standard data for Cu_2Sb (tetragonal structure, powder diffraction file pdf: 3-1023). The same match with this standard was observed for the precursor deposited onto glass substrates. The lattice parameters for the Cu_2Sb phase were calculated to be a = b = 4.015 Å and c = 6.108 Å in good agreement with the reference data.

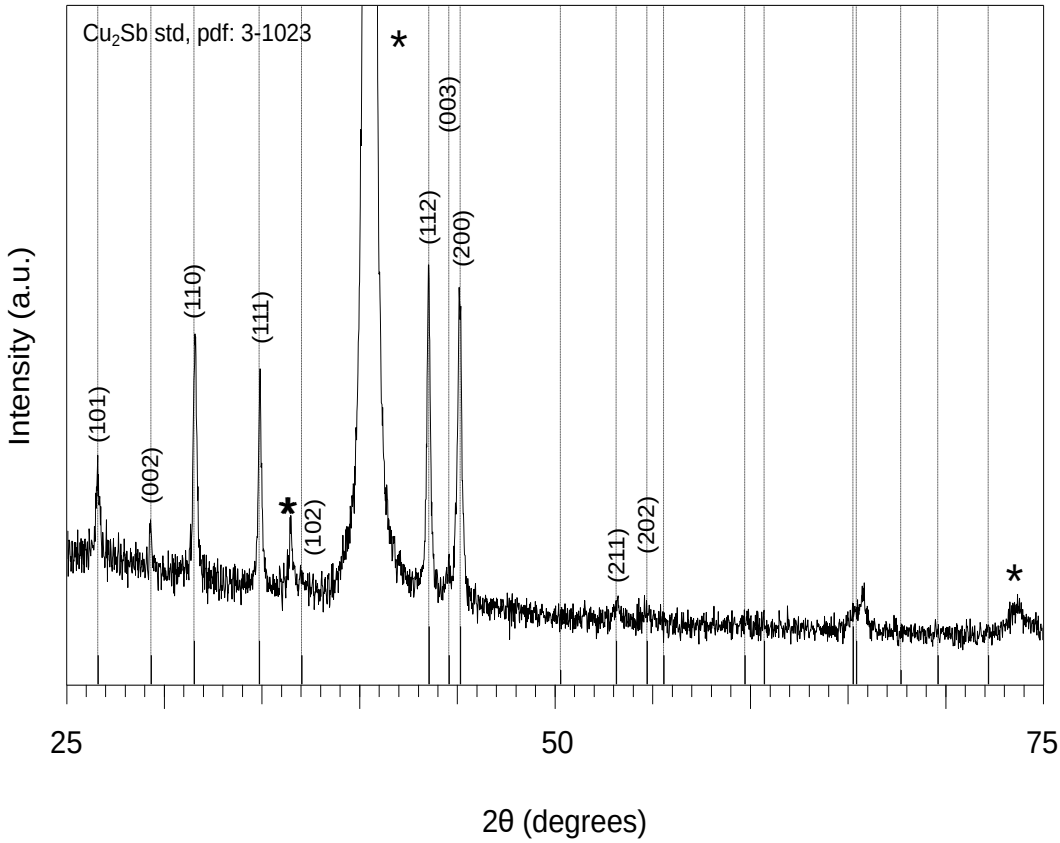

Figure 1. XRD pattern of metallic Cu-Sb precursor deposited on Mo/SLG substrate, showing good agreement with the standard XRD pattern for Cu_2Sb tetragonal lattice (pdf: 3-1023, vertical lines). The * symbols indicate the position of the Mo substrate peaks.

3.2 Sulphurisation of Cu-Sb precursors

Materials characterisation

The metallic precursor films were sulphurised using elemental sulphur powder for seven different temperatures between 250-550 °C in 50 °C steps. The absorber layers annealed at 250 °C, 300 °C and 500 °C exhibited good adhesion on both the Mo/glass and glass substrates. Poor adhesion was observed for the samples treated at 350 °C and 400 °C, this was possibly associated with Cu_3SbS_3 phase evolution at these temperatures (as detailed in the next paragraph). Complete evaporation of the film was observed at 550 °C. A rough surface was observed for all the samples except for the film sulphurised at 500 °C.

Figure 2 shows the XRD patterns collected for the films deposited on glass substrates, converted at 250 °C, 300 °C and 350 °C together with the standard powder pattern for Cu_3SbS_3 (cubic structure, pdf: 075-1574). Peaks matching the standard XRD patterns of CuS and Sb_2S_3 (pdf: 079-2321 and 002-0374, respectively – not displayed for clarity) are observed for the samples sulphurised at 250 °C and 300 °C, indicating the formation of a mixture of CuS and Sb_2S_3 phases at these temperatures. The XRD spectrum for the sulphurised film at 350 °C exhibits a clear change in phase, with formation of a predominant Cu_3SbS_3 phase (pdf: 075-1574). A secondary $CuSbS_2$ phase was also identified at this temperature. However the nearly complete disappearance of chalocostibite ($CuSbS_2$ pdf: 044-1417) indicated by the dotted areas of Figure 3 indicates that a temperature of at least 500 °C is required for the formation of a strongly dominant Cu_3SbS_3 phase. As the temperature increases the disappearance of the secondary phases coincides with an increase in Cu_3SbS_3 peak intensities.

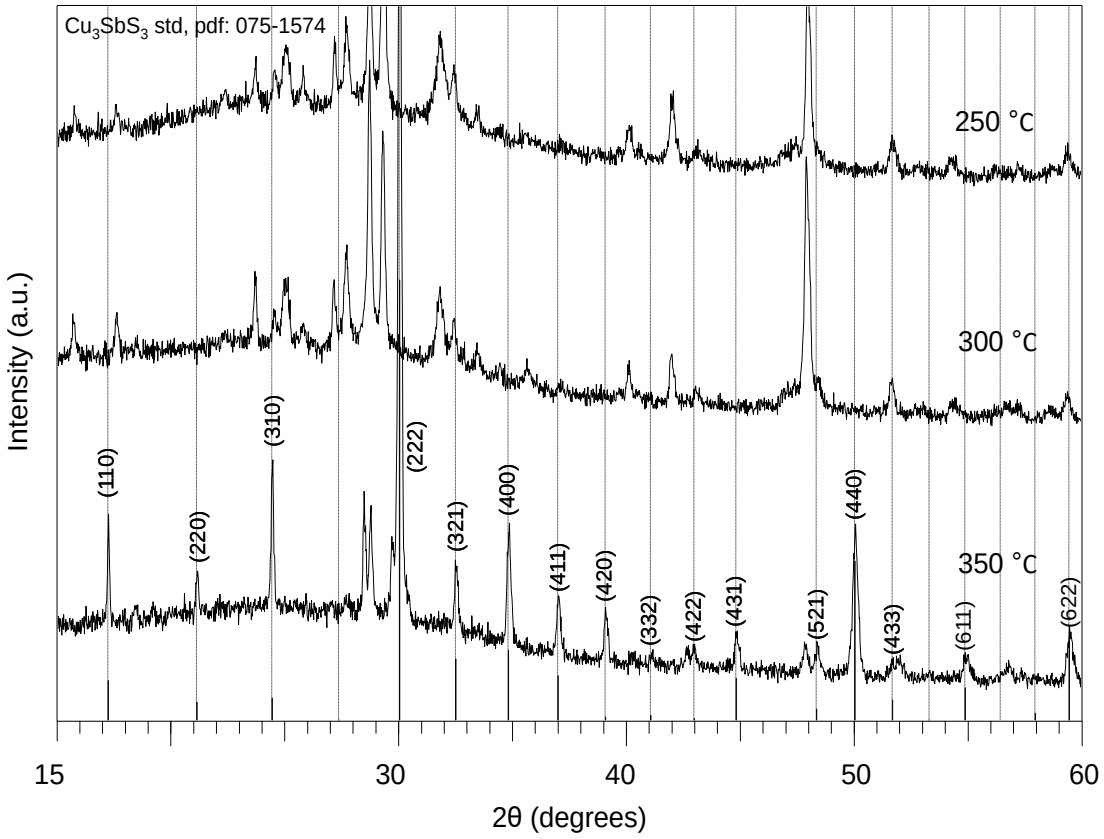

Figure 2. XRD patterns of Cu-Sb precursor films deposited on glass substrates sulphurised (with sulphur powder) at 250°C, 300°C and 350°C. A clear transition of phase can be noticed between the films converted at 300 °C and 350 °C. The sample sulphurised at 350 °C shows a good match with the standard XRD powder pattern for the cubic structure of Cu_3SbS_3 (pdf: 075-1574).

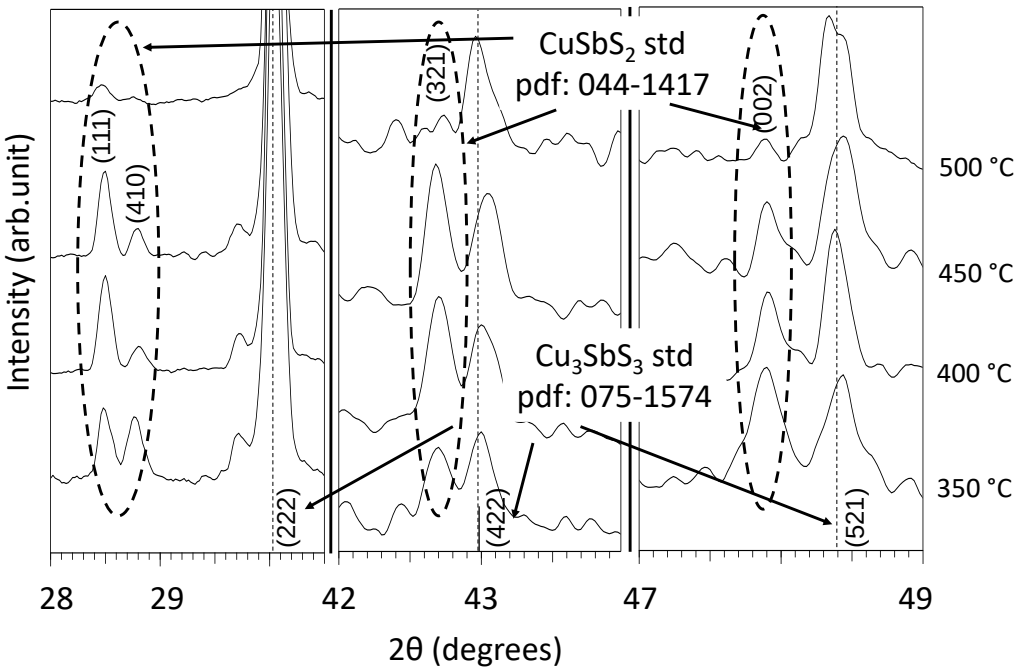

Figure 3. Part-XRD patterns of films processed at 350-500 °C on glass substrates using sulphur powder. The three different areas of the spectrum show the disappearance of peaks associated with $CuSbS_2$ (circled peaks, chalcostabite pdf: 044-1417) with the increase of temperature. Peaks related to the Cu_3SbS_3 (dotted straight lines, pdf: 075-1574) remain stable and their height and sharpness increase with temperature, indicating that at least a temperature of 500 °C is required for the formation of a strongly dominant Cu_3SbS_3 phase.

Precursors processed on glass substrates at temperatures higher than 300 °C showed a predominant Cu_3SbS_3 cubic phase (Figure 4 (a), pdf: 075-1574) while a Cu_3SbS_3 monoclinic phase was observed for the films deposited on Mo/glass substrates (Figure 4 (b), pdf: 083-0563). This could indicate that the molybdenum, in particular, and more generally, the substrate has an influence on the subsequent film structure. However the predominant transition to a Cu_3SbS_3 phase for temperatures higher than 300 °C remained clear for films grown on both glass and Mo/glass substrates, notwithstanding the different Cu_3SbS_3 structures.

In order to obtain greater control over the sulphurisation process a 1.5 µm layer of elemental sulphur was evaporated directly onto the precursor instead of using elemental sulphur powder before conversion at 500 °C. The film produced using the evaporated sulphur layer was adherent to the substrate and exhibited an XRD pattern that was in good agreement with the standard XRD pattern for Cu_3SbS_3 (monoclinic system pdf: 083-0563, figure 4 (c)). Of the conversion temperatures used, the optimum temperature was determined to be 500 °C, either on glass or Mo/glass substrate. However the use of different substrates led to the formation of two substantially different film structures for the same experimental conditions used.

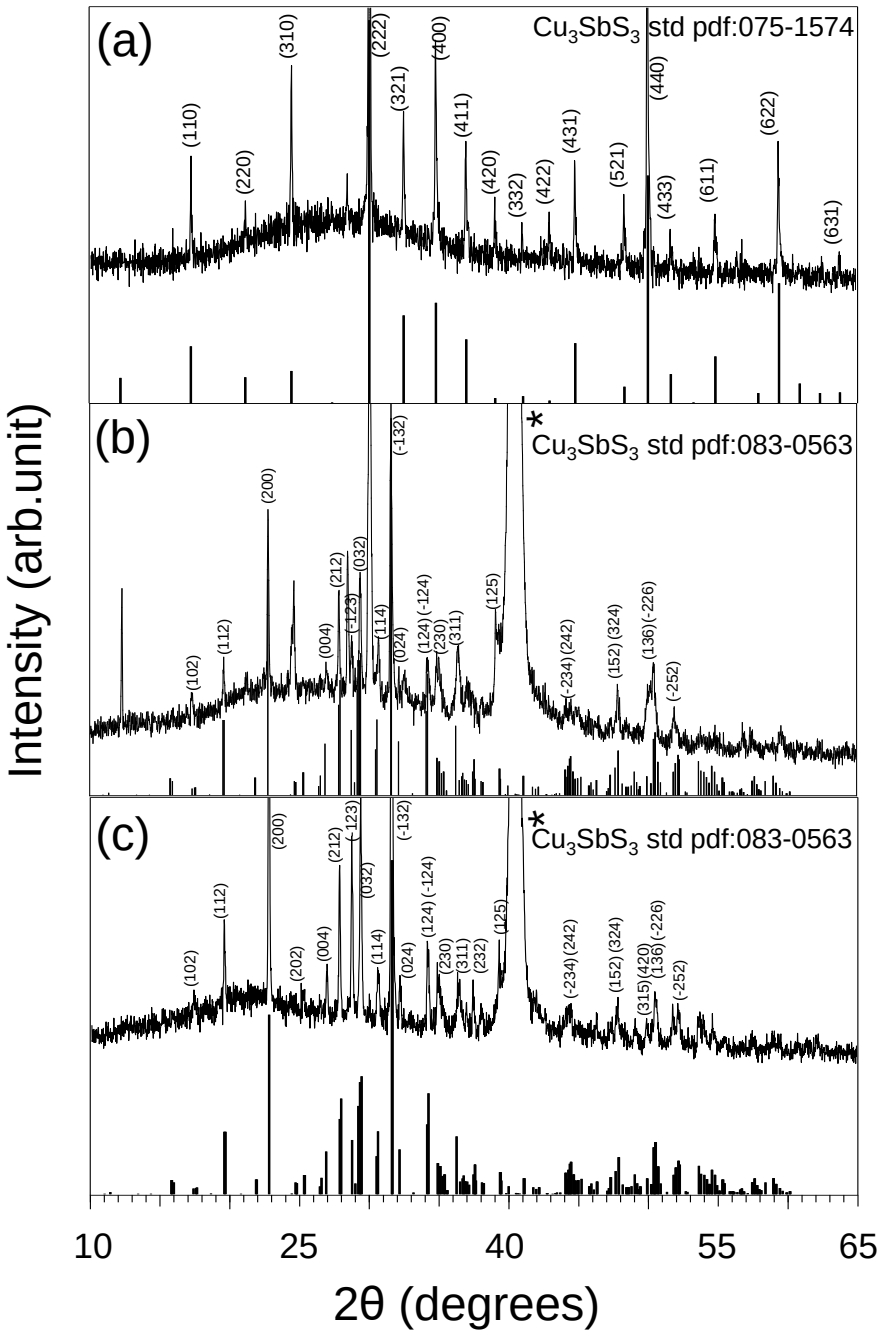

Figure 4. XRD patterns of films processed at 500 °C with: (a) sulphur powder on SLG substrate; (b) sulphur powder on Mo/SLG substrate, (c) evaporated sulphur on Mo/SLG substrate. Standard patterns for a) Cu_3SbS_3 (cubic structure, pdf: 075-1574) and (b-c) Cu_3SbS_3 pdf: 083-0563 (Skinnerite – synthetic monoclinic) are also included. The * symbols indicate the position of the Mo substrate peak.

SEM micrographs of the precursor layers (on glass substrate) sulphurised at different temperatures are shown in Figure 5. The samples sulphurised at 250 and 300 °C consist of needle-like crystallites. At 250 °C (Figure 5 (a)) the needles are uniformly distributed onto the surface forming a bulk structure with voids of size 0.2-0.5 µm. The sample converted at 300 °C (Figure 5 (b)) shows more compact and thinner needles grouped in 1-1.5 µm large star shaped clusters. For conversion temperatures higher than 300 °C (Figure 5 (c-f)) the morphology of the films changes significantly. The needle-like shape of the crystallites disappears at these temperatures changing into a bulk granular surface, with a more densely packed structure. For the films converted at 400 and 450 °C (Figure 5 (d-e)) a uniform surface can be observed, whereas at 350 and 500 °C (Figure 5 (c,f)) spread particles in a 0.5-1.5 µm range uniformly cover the bulk porous surface. However significant differences in shape can be observed between the particles of the two samples, being almost flakes at 350 °C and more rounded at 500 °C. This implies a different structure and composition of the particles, although further and more detailed analysis should be carried out in order to prove it. The sharp morphological changes observed between 250 °C and 300 °C correlates well with the XRD observations reported earlier and the change in colour of the samples from dark blue to light grey.

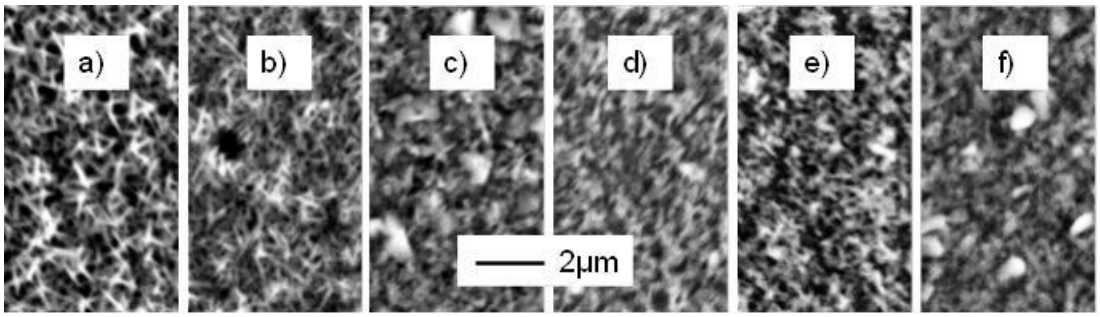

Figure 5. Surface SEM micrographs of the sulphurised samples at (a) 250 °C (b) 300°C (c) 350°C (d) 400°C (e) 450°C (f) 500°C using elemental S powder.

Depth profiles of the elements acquired by SIMS for a Cu_3SbS_3/Mo film are plotted in Figure 6. The data is shown for a film that was sulphurised at 500 °C using an evaporated sulphur layer. The profiles shows a Sb gradient at the near surface region of the film indicating a slightly Sb-poor surface. This coincides with the S profile which shows a gradient in the opposite direction, implying a slightly S-rich content. This is possibly due to the formation of CuS_x phase at the near surface of the specimen [17]. In general all the elements are seen to be uniform throughout the film depth, indicating a full conversion of the Cu-Sb precursor during the sulphurisation process. Note that the extension of the ^{121}Sb signal into the Mo layer is due to an interference with another cluster ion of mass 121, i.e. $^{23}Na^{98}Mo$.

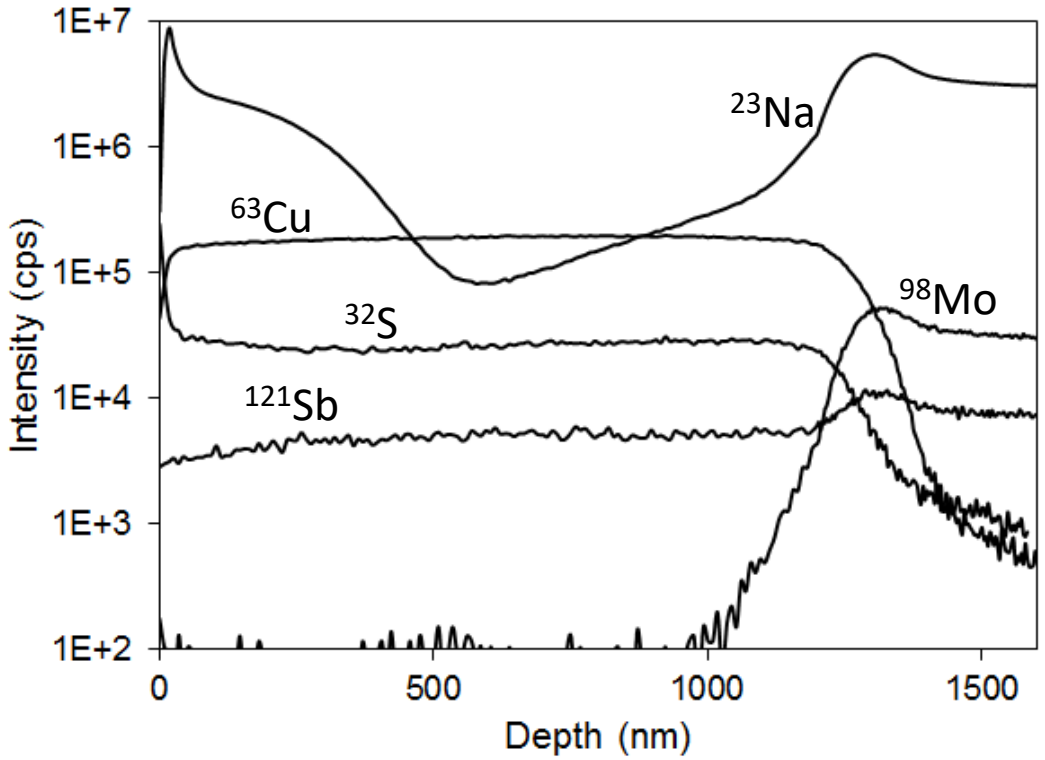

Figure 6. SIMS depth profiles for a Cu_3SbS_3/Mo film sulphurised at 500 °C with sulphur evaporated on the metallic precursor.

A comparison of SEM micrographs for sulphurised precursors at 500 °C is shown in Figure 7. EDS compositional data are also reported in Table 1. Figure 7 (a-b) shows the surface of sample converted using evaporated sulphur. Figure 7 (c) shows a micrograph of the precursor converted with sulphur powder. The use of different sulphurisation techniques lead to a substantial change of morphology of the surface. The film appears to be cracked with small grains when evaporated sulphur is used, while a film processed with sulphur powder shows larger grains of 2 types: the main part of the film has similar aspect to Figure 7 (a) but there is also the growth of another type of very ordered and elongated grains. Individual smooth grains in the 2-10 μm range can be observed. EDS analysis of the samples (Table 1) indicates that the measured stoichiometry of the produced film processed with sulphur evaporation technique is close to Cu_3SbS_3. Assuming uniform elemental distributions this yields the compound $Cu_{3.0}Sb_{1.2}S_{2.9}$. The film fabricated with sulphur powder resulted in a sulphur rich composition. No clear stoichiometry could be identified for this layer, confirming the mixture of phases observed in the XRD analysis. The overlapping of the Mo and S energy peaks in the EDS analysis is considered to be negligible, since the thickness of all the processed films (about 1.2 μm) is sufficient to avoid the detection of the Mo substrate.

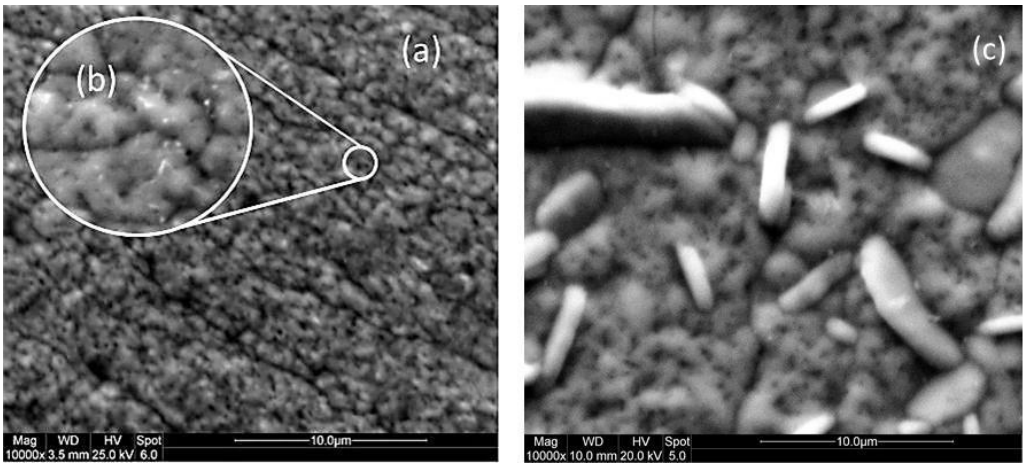

Figure 7. SEM micrographs of sulphurised Cu-Sb precursors at 500 °C on Mo/SLG substrates: (a) with evaporation technique, (b) at higher magnification and (c) with powder technique.

	Cu (at%)	*Sb (at%)*	*S (at%)*
Cu-Sb precursor	68.3	31.6	//
Sulphurised precursor with evaporated S	42.5	16.5	41.0
Sulphurised precursor with S powder	30.3	15.3	54.4
Ideal stoichiometry of Cu_3SbS_3	42.9	14.3	42.9

Table 1. EDS analysis of the Cu-Sb metallic precursor and the corresponding sulphurised layer at 500 °C with evaporated sulphur and sulphur powder (the last row shows the ideal stoichiometry for Cu_3SbS_3).

Electrical and Optoelectronic Characterisation

Electrolyte/absorber junctions formed with the films deposited on Mo/glass were used to check for photo-activity under pulsed white illumination using the three electrode configuration described in section 2. A p-type conductivity was also detected with the electrochemical analysis. The film converted at 500 °C using evaporated sulphur in the conversion process, was the only one found to be photo-active. None of the films produced at lower temperatures (on Mo/glass) utilising powder in the conversion, exhibited photo-activity. The photo-active sample was further characterised using the electrochemical technique to measure the external quantum efficiency spectrum, shown in Figure 8 (a). The fabricated layer showed a weak quantum yield of 0.5%-4% in the photon range of 1.8 – 3.0 eV.

For an ideal Schottky barrier electrolyte junction, the relation between the external quantum efficiency and the absorption coefficient α is given by [18]:

$EQE = 1 - \exp(-\alpha w)$

where w is the width of the space charge region. Since the absorption of photons occurs in films about 1 µm thick, the type of electronic transition can be considered direct. For allowed direct transitions, the dependence of the absorption coefficient on photon energy is given by [19]:

$\alpha h\nu \propto (h\nu - E_g)^{1/2}$

where $h\nu$ is the photon energy and E_g is the energy bandgap of the semiconductor.

Therefore a plot of $[h\nu \ln(1-EQE)]^2$ as function of photon energy is linear for energies greater than E_g, with the intercept yielding the value of the bandgap E_g. The calculated bandgap is 1.84 eV for the Cu_3SbS_3 film as shown in Figure 8 (b).

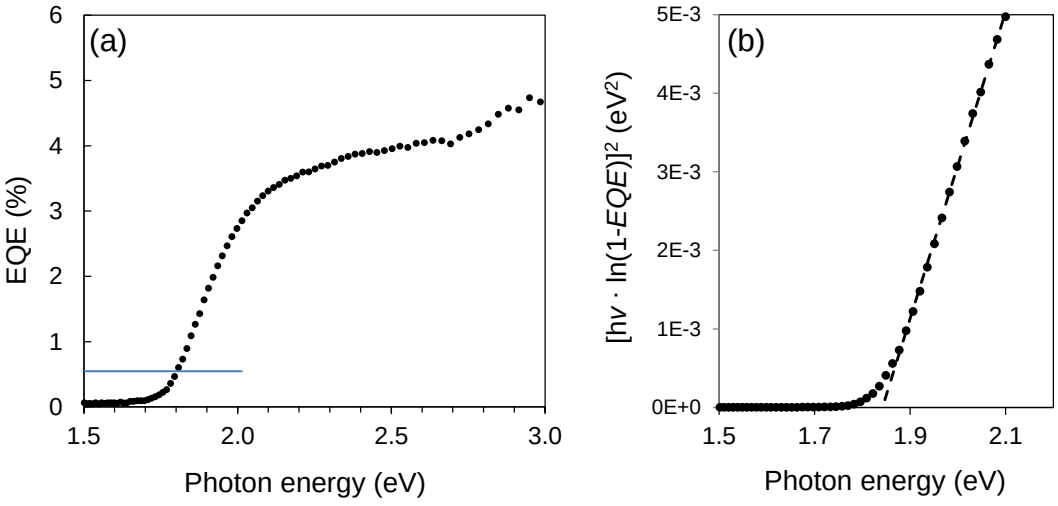

Figure 8. (a) EQE plot for the semiconductor/electrolyte interface related to a photo-active film sulphurised at 500°C with sulphur evaporated on the metallic precursor, measured at -0.8V vs. Ag|AgCl in 0.2 M $Eu(NO_3)_3$ and (b) $[h\nu \ln(1-EQE)]^2$ versus $h\nu$ plot of the layer, the extrapolation yields an energy bandgap value of 1.84 eV.

In conclusion two different sulphurisation techniques were tested, based on the sulphur introductory method in the reaction chamber prior the heating process. This was achieved by (i) the use of elemental powder or (ii) the evaporation of sulphur layer onto the metallic precursors. It was found that a temperature of at least 300 °C is required to form the ternary Cu_3SbS_3 compound crystallising in the cubic structure for glass substrates with (i) and in a monoclinic lattice for glass and Mo/glass substrate with either (i) or (ii). However a temperature of 500 °C is required for a dominant ternary phase to be detected. Under those conditions film processed with (ii) shows photo-activity with an electronic bandgap of 1.84 eV.

3.3 Combined sulphurisation/selenisation of Cu-Sb precursors

The photo-active Cu_3SbS_3 films sulphurised at 500 °C using the sulphur evaporation technique showed a bandgap of 1.84 eV and p-type conductivity, making this material promising for photovoltaic solar applications. However theoretical calculations carried out by Loferski [20] showed that a bandgap in the range of 1.4-1.6 eV is sought for optimal conversion efficiency in single junction solar cells, for terrestrial applications. Looking at the behaviour of similar chalchogenide compounds, it was expected that sulpho-selenides of Cu-Sb metallic precursors would exhibit energy bandgap values lower than the corresponding sulphides, as in the case of $CuSb(Se,S)_2$, $CuIn(Se,S)_2$, $Cu(InGa)(S,Se)_2$ and $Cu_2ZnSn(Se,S)_4$ [14, 21-23]. In order to reduce the energy bandgap of Cu_3SbS_3, a combined selenisation and sulphurisation experiment was performed. A series of precursors was coated with a layer of selenium followed by a layer of sulphur, before annealing at 500 °C in argon ambient. The thicknesses of the Se and S layers were chosen to yield a range of compounds. The Se/S thickness ratios used in the chalcogenisation process are reported in Table 2. Pure selenisation of the precursors without presence of sulphur was also attempted. The produced films did not show any formation of Cu_3SbSe_3 or $CuSbSe_2$ phases and only mixtures of multiple phases could be detected.

Se layer (nm)	*S layer (nm)*	*Se/S thickness ratio*
55	560	0.1
530	540	1
560	55	10

Table 2. Thicknesses of evaporated chalcogen onto the precursors used in the combined S/Se conversion process. The S layer is evaporated on top of the Se layer.

Materials Characterisation

A stoichiometry to $Cu_3Sb(Se_xS_{1-x})_3$ compound appears in the atomic composition analysis as reported in Table 3. The content of Cu, Sb and S+Se changes marginally, remaining close to the $Cu_3Sb(Se_xS_{1-x})_3$ stoichiometry. On the other hand wide variations of S and Se can be observed, indicating their mutual substitution, according to the Se/S thickness ratio used in the process.

Se/S thickness ratio	*Cu(at%)*	*Sb(at%)*	*Se(at%)*	*S(at%)*	*(Se+S)(at%)*	*x*
10	42.0	17.3	19.8	20.8	40.7	0.49
1	40.0	15.5	13.4	26.2	39.6	0.34
0.1	41.0	17.1	3.3	38.6	41.8	0.08
0 (only S)	42.5	16.5	//	41.0	41.0	0

Table 3. Atomic composition analysis of the sulphur/selenised films. The first column shows the Se/S thickness ratios used during the chalcogenisation process.

The XRD powder patterns of the films converted with three different Se/S thickness ratios show a mixture of different phases for all the converted films. However the $Cu_3Sb(Se_xS_{1-x})_3$ structure (monoclinic system pdf: 083-0563), is the predominant phase in all the analysed patterns. The top section of figure 9 shows the XRD spectra for films with x=0.34 (top spectrum) and x=0 (bottom spectrum). For x=0.34 secondary phases are present in the films, each with different values of x (not shown). These secondary phases were not detected for the pure sulphide film. The evolution of selected XRD peaks as a function of x is shown at the bottom section of figure 9. As the Se content increases the diffracted peaks shift towards smaller diffraction angles indicating a reduction in lattice parameter in accordance with sulphur substitution by selenium. It is also noted that the peak intensity and width varies and this could indicate either the presence of additional phases or an incomplete conversion process. The calculations of lattice parameters reported in Table 4 shows a linear decrease of the parameter a when x increases. However the variation of both b and c parameters could not be correlated to the composition of the film.

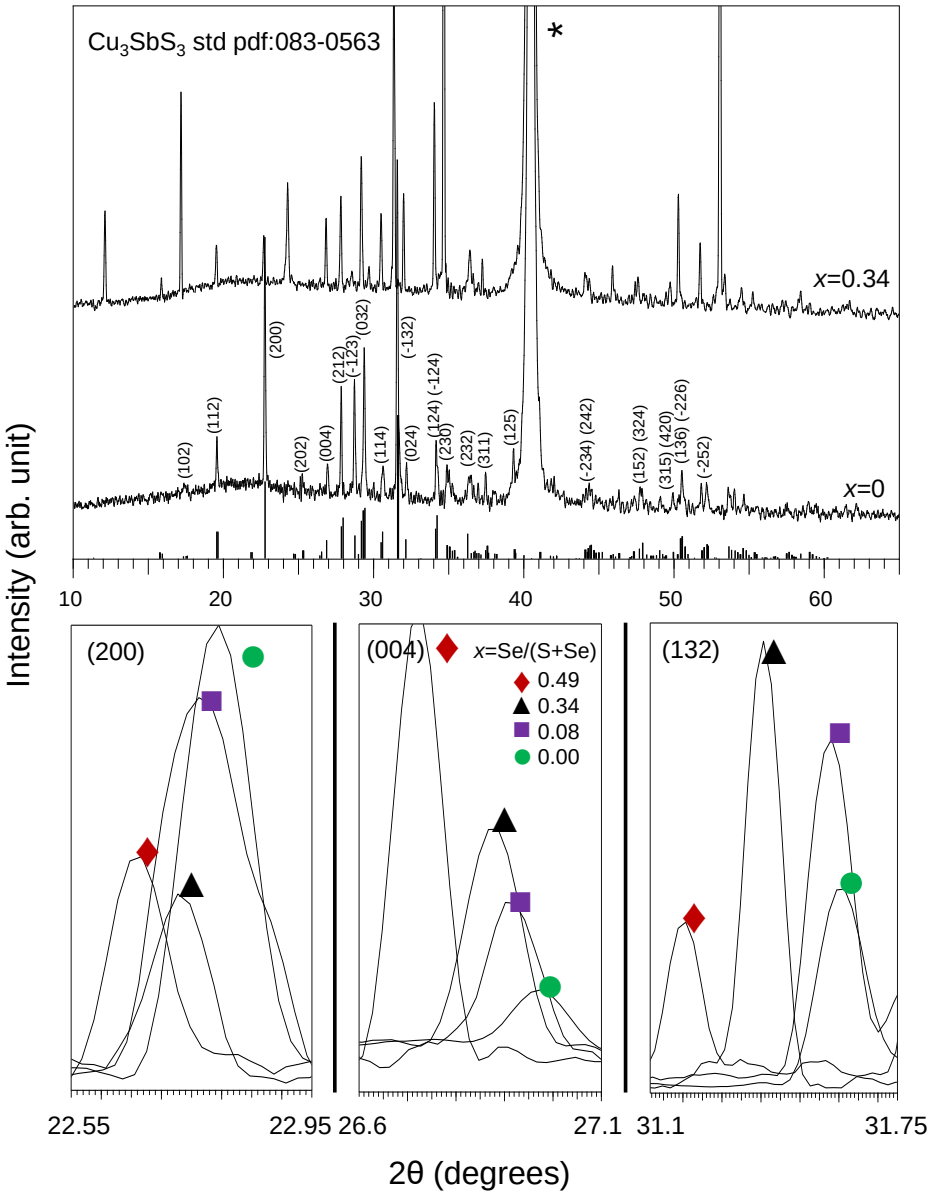

Figure 9. Top: XRD spectra for films with a Se/(Se+S) atomic ratio of *x*=0.34 (top spectrum) and *x*=0 (bottom spectrum). Bottom: part-XRD patterns of sulpho-selenides films processed at 500°C. Each panel shows the shift of one particular peak as a function of x. The Miller indices of each peak is reported on the top left side of each panel. The * symbol indicates the position of the Mo substrate peak.

Table 4 shows the evolution of the crystallite size as function of *x* as determined using Scherrer's formula [24] applied to the (132) x-ray reflections. For 0<x<0.34 the crystallite size increases monotonically with x but a drop is observed for x=0.49. For this value the corresponding XRD

spectrum shows an increase of other unidentified phases. The high Se content involved for this particular conversion could start to inhibit further incorporation of Se into the structure preventing the formation of a single phase material. This could explain the inconsistency with the trend observed for higher content of Se.

x=Se/(Se+S)	*E_g (eV)*	*Crystal size from (132) (nm)*	*Lattice parameter a (Å)*	*Lattice parameter b (Å)*	*Lattice parameter c (Å)*
0.49	1.38	83	7.73	10.30	13.10
0.34	1.42	107	7.75	10.30	13.22
0.08	1.80	103	7.79	10.28	13.18
0	1.84	70	7.81	10.29	13.17

Table 4. Bandgap values, lattice parameters and crystal sizes as a function of *x*.

Figure 10 (a) depicts the cross section SEM image of a film with x=0.34 which shows large grains extending the full thickness of the film. Figure 10 (b) shows the corresponding SIMS depth profiles. At the near surface of the film a sharp variation is observed for almost all the detected ions except for ^{121}Sb. Such variations are explained by the oxidation state of the film surface. However after etching this upper part of the film, the count of Cu, Sb, S and Se becomes more stable with a slight decrease of Cu and a gentle rise of S and Se. A sharp decrease of all the elements can be noticed when the Mo substrate is reached. The only element that remains stable after the Mo/semiconductor interface is ^{121}Sb, this is due to a mass interference as explained in the section 3.2. The analysis shows a good uniformity throughout the thickness of the converted layer demonstrating full reaction of the Cu-Sb metallic layer with the chalcogens during the conversion process.

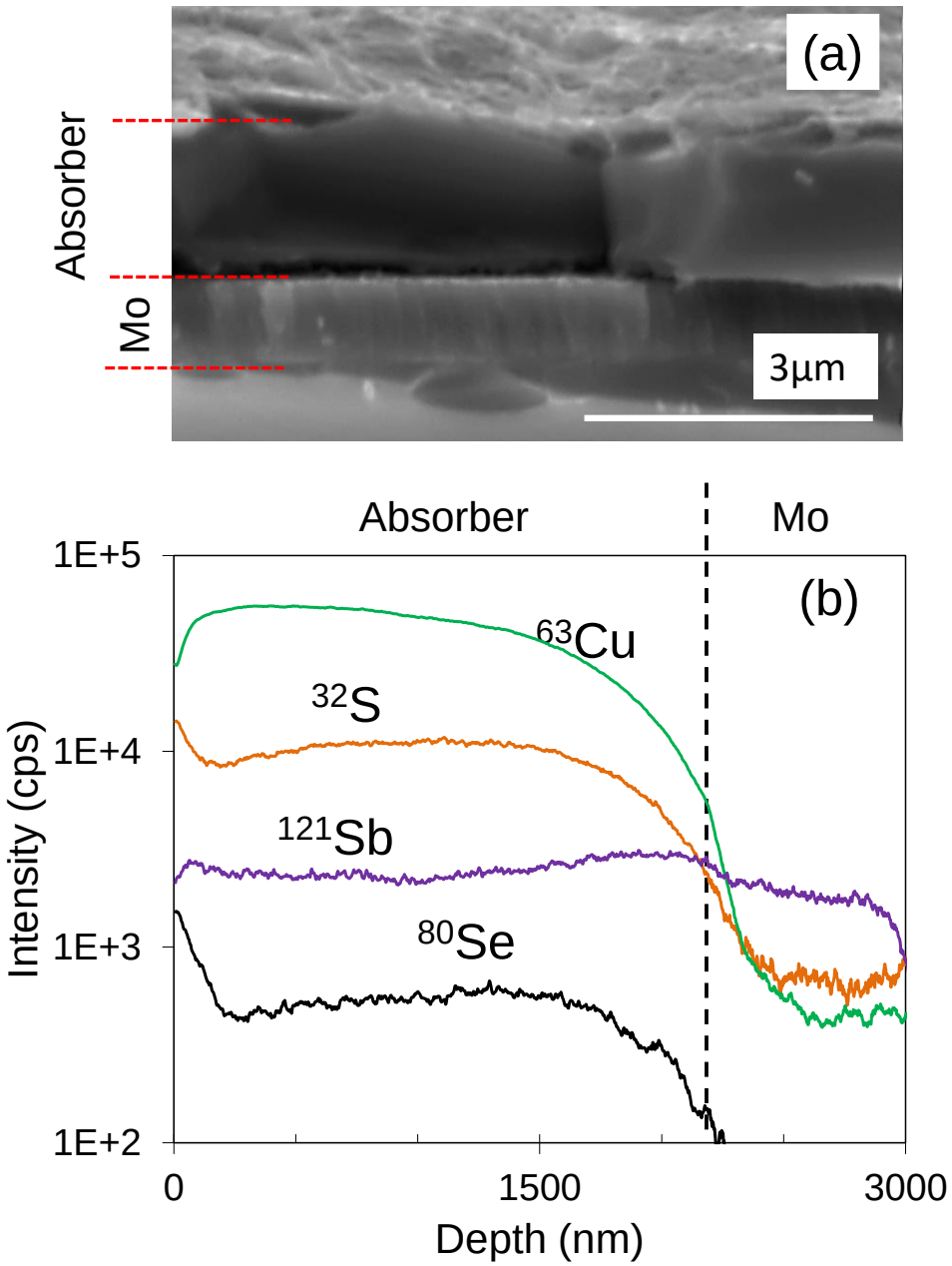

Figure 10. (a) SEM cross section image for a film with *x*=0.34 and energy band gap of 1.42 eV. (b) SIMS depth profiles of the same film.

Junction and Devices

The $Cu_3Sb(Se_xS_{1-x})_3$ films resulted in several compounds which were p-type and photo-active and their photoresponses expressed as quantum efficiency in the Eu^{3+} electrolyte, are shown in Figure 11 (a). The EQE values were similar in magnitude for all films at between 3-5%. The low response of the films is likely to result from the films being non-optimal, and further optimisation is required to improve the properties to ensure they are single

phase and that the number of process-related pinholes is minimised. An important feature that can be seen from the data is that the onset of EQE for each sample is shifted towards lower energy values as *x* increases. This indicates that the absorption edge is moving towards lower energy values with the increase of selenium content. The energy bandgap of each film was determined using equation 2 and the associated plots are shown in Figure 11 (b).

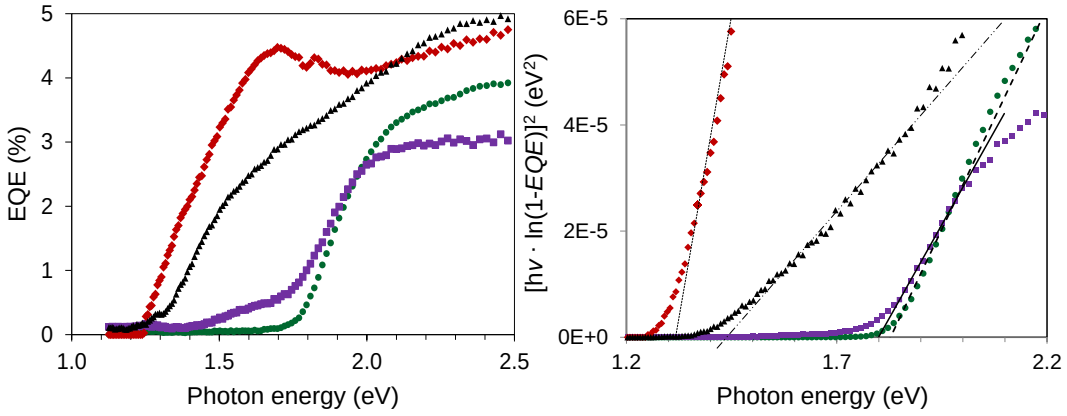

Figure 11. (a) EQE plots of sulpho-selenides films measured at -0.8V vs. Ag|AgCl in 0.2 M $Eu(NO_3)_3$ as a function of photon energy for several values of *x*. (b) **.** [h*v* * ln(1-*EQE*)]^2 plots as a function of incident photon energy for films annealed with different values of *x*. The straight lines intercept with the x-axis yields the electronic energy bandgap of each film. The analysis is based on the assumption that the processed films are direct bandgap material.

Figure 11 (b) and Table 3 indicate that the energy bandgap of the films varied between 1.84 eV for the pure sulphide to 1.32 eV for the film with the highest Se content (x=0.49). The variation of bandgap as a function of the *x* as determined by EDS is shown in Figure 12. The trend is a linear reduction in bandgap as the Se content in the film increases. This trend can be extrapolated to determine the energy bandgap of the film for x=1, i.e. Cu_3SbSe_3, and this would be 0.71 eV.

.

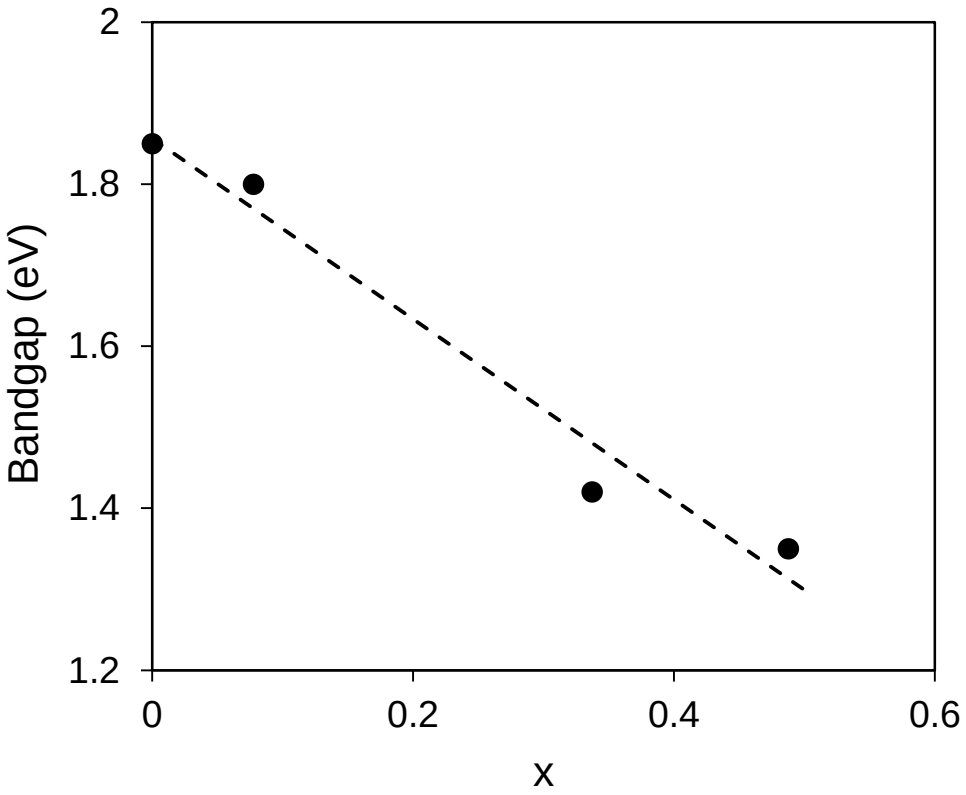

Figure 12. Evolution of energy bandgap for $Cu_3Sb(Se_xS_{1-x})_3$ films as a function of x

The absorber layers had demonstrated photoactivity using electrolyte/absorber junctions. To further investigate their suitability for photovoltaic applications, selected layers were incorporated into devices. The photo-active layers were subsequently made into devices using the conventional structure: Ni-Al(50-3000 nm)/ITO(180 nm)/i-ZnO (60 nm)/CdS(50 nm)/absorber/Mo (850 nm)/glass(1 mm) substrate design used for CIGS solar cells. The total area of the produced cells was 25 mm^2. The similarities of the films to other chalcogenides indicated that the use of this cell structure would be suitable as a starting point for the layers. No optimisation for buffer layers was undertaken. Cells using the absorber layer with *x*=0.08 and a band-gap of 1.80 eV, exhibited photovoltaic behaviour with values of open circuit voltage and short circuit current density in the ranges 1-3.5 mV and 1.0-1.6 $mA \cdot cm^{-2}$, respectively. The remaining cells produced using absorbers with different values of *x* were inactive under illumination. It is expected that with further absorber layer and device optimisation the photovoltaic performance of these devices will improve and that all films

exhibiting photo-activity in the electrolyte/absorber junction configuration will also show photovoltaic behaviour.

4. Conclusions

The synthesis of $Cu_3Sb(Se_xS_{1-x})_3$ thin films was achieved by sputtering Cu-Sb metallic precursors onto either glass or Mo/glass substrates and then reacting the precursors with either sulphur, or a mixture of sulphur and selenium. In the case of Se-free films (x=Se/(Se+S)=0) the results indicated that the use of a controlled evaporation of a layer of sulphur instead of simple powder facilitated the formation of a predominant Cu_3SbS_3 monoclinic phase which had improved adhesion to the substrate. The pure sulphide films produced from precursor layers deposited on Mo/glass and converted at 500 °C using the sulphur evaporation technique showed a p-type conductivity and a photo-response when exposed to light that enabled an energy bandgap of 1.84 eV to be measured. The electronic properties of the films could be adjusted by introducing a controlled amount of Se with the resulting films converted at 500 °C being photo-active. P-type conductivity and energy bandgaps between 1.84 and 1.38 eV were observed for $0<x<0.49$. This series of photo-active films was incorporated and tested in a typical Ni-Al/ITO/i-ZnO/CdS/absorber/Mo/Glass solar cell structure. The cell based on the absorber layer corresponding to x=0.08 and a band-gap of 1.80 eV exhibited a measureable photovoltaic response with maximum values of open circuit voltage and a short circuit current density of 3.5 mV and 1.6 $mA \cdot cm^{-2}$ respectively. It is believed that this may be the first report of a functioning photovoltaic device based on a $Cu_3Sb(Se,S)_3$ absorber layer.

Given the relative abundance of the constituent elements, which are also non-toxic, $Cu_3Sb(Se_xS_{1-x})_3$ might be an interesting ternary compound for making low cost thin film solar cells.

.

Acknowledgements

The authors acknowledge support of the UK Engineering and Physical Sciences Research Council SUPERGEN Initiative for the program ‘PV-21’.

References

[1] R. W. Miles, G. Zoppi, I. Forbes, Inorganic Photovoltaic Cells, Materials Today, 10 (2007) 20-27.
[2] M.A. Green, K. Emery, Y. Hishikawa, W. Warta, Solar cell efficiency tables (version 36), Progress in Photovoltaics: Research and Applications, 18 346-352.

[3] W.G.J.H.M. van Sark, G.W. Brandsen, M. Fleuster, M.P. Hekkert, Analysis of the silicon market: Will thin films profit?, Energy Policy, 35 (2007) 3121-3125.
[4] F. A. Feltrin, Material Challenge fro Terawatt Level Deployment of Photovoltaics, Photovoltaic Energy Conversion, Conference Record of the 2006 IEEE 4th World Conference, 2 (2006) 2496-2472.
[5] H. Dittrich, A. Bieniok, U. Brendel, M. Grodzicki, D. Topa, Sulfosalts — A new class of compound semiconductors for photovoltaic applications, Thin Solid Films, 515 (2007) 5745-5750.
[6] H. Dittrich, A. Stadler, D. Topa, H.-J. Schimper, A. Basch, Progress in sulfosalt research, physica status solidi (a), 206 (2009) 1034-1041.
[7] M.E. Nell, A.M. Barnett, The spectral p-n junction model for tandem solar-cell design, International Electron Devices Meeting 34 (1987) 257-266.
[8] T.J. Coutts, J.S. Ward, D.L. Young, K.A. Emery, T.A. Gessert, R. Noufi, Critical issues in the design of polycrystalline, thin-film tandem solar cells, Progress in Photovoltaics: Research and Applications, 11 (2003) 359-375.
[9] D. Colombara, L.M. Peter, K.D. Rogers, J.D. Painter, S. Roncallo, Formation of CuSbS2 and CuSbSe2 thin films via chalcogenisation of Sb–Cu metal precursors, Thin Solid Films, 519 (2011) 7438-7443.
[10] C. Garza, S. Shaji, A. Arato, E. Perez Tijerina, G. Alan Castillo, T.K. Das Roy, B. Krishnan, p-Type CuSbS2 thin films by thermal diffusion of copper into Sb2S3, Solar Energy Materials and Solar Cells, 95 (2011) 2001-2005.
[11] A. Rabhi, M. Kanzari, B. Rezig, Growth and vacuum post-annealing effect on the properties of the new absorber CuSbS2 thin films, Materials Letters, 62 (2008) 3576-3578.
[12] Y. Rodríguez-Lazcano, M.T.S. Nair, P.K. Nair, CuSbS2 thin film formed through annealing chemically deposited Sb2S3–CuS thin films, Journal of Crystal Growth, 223 (2001) 399-406.
[13] Y. Rodríguez-Lazcano, L. Guerrero, O. Gomez Daza, M. T. S. Nair, P.K. Nair, Antimony chalcogenide thin films: chemical bath deposition and formation of new materials by post deposition thermal processing, Superficies y Vacío, 9 (1999) 100-103.
[14] J. Zhou, G.-Q. Bian, Q.-Y. Zhu, Y. Zhang, C.-Y. Li, J. Dai, Solvothermal crystal growth of CuSbQ2 (Q=S, Se) and the correlation between macroscopic morphology and microscopic structure, Journal of Solid State Chemistry, 182 (2009) 259-264.
[15] Maiello P., Zoppi G., Hutchings K., S. Roncallo, Miles R. W., Forbes I., Cu-Sb library for solar cell absorber material identification, Proceedings of 8th Photovoltaic Science Applications and Technology (PVSAT-8), (2012) 137-140.
[16] P. J. Dale, A. P. Samantilleke, G. Zoppi, I. Forbes, S. Roncallo, L.M. Peter, Deposition and Characterization of Copper Chalcopyrite Based Solar Cells using Electrochemical Techniques, 211th ECS Transactions, 6 (2007) 535-546.
[17] Y. B. He, A. Polity, R. Gregor, D. Pfisterer, I. Österreicher, D. Hasselkamp, and B. K. Meyer, "Characterization of RF reactively sputtered Cu–In–S thin films," *Physica B: Condensed Matter,* vol. 308–310, pp. 1074-1077, 2001.

[18] J.J. Scragg, P.J. Dale, L.M. Peter, G. Zoppi, I. Forbes, New routes to sustainable photovoltaics: evaluation of Cu2ZnSnS4 as an alternative absorber material, physica status solidi (b), 245 (2008) 1772-1778.
[19] J.I. Pankove, Optical Processes in Semiconductors, Prentice Hall, Englewood Cliffs NJ, 1971.
[20] J. Loferski, Theoretical Considerations Governing the Choice of the Optimum Semiconductor for Photovoltaic Solar Conversion, Journal of Applied Physics, 27 (1956).
[21] R. Yoosuf, M.K. Jayaraj, Study on sulfur diffusion in CuInSe2 thin films using two thermal profiles, Thin Solid Films, 515 (2007) 6188-6191.
[22] M. Turcu, I. M. Kötschau, U. Rau, Composition dependence of defect energies and band alignments in the $Cu(In_{1-x}Ga_x)(Se_{1-y}S_y)_2$ alloy system, Journal of Applied Physics, 91 1391.
[23] Q. Guo, G.M. Ford, W.-C. Yang, B.C. Walker, E.A. Stach, H.W. Hillhouse, R. Agrawal, Fabrication of 7.2% Efficient CZTSSe Solar Cells Using CZTS Nanocrystals, Journal of the American Chemical Society, 132 (2010) 17384-17386.
[24] G. Zoppi, N. Beattie, J. Major, R. Miles, and I. Forbes, "Electrical, morphological and structural properties of RF magnetron sputtered Mo thin films for application in thin film photovoltaic solar cells," *Journal of Materials Science,* vol. 46, pp. 4913-4921, 2011